A&A 509, A98 (2010)
DOI: 10.1051/0004-6361/200913350

Astronomy & Astrophysics

Modelling line emission of deuterated H_3^+ from prestellar cores

O. Sipilä[1,3], E. Hugo[2], J. Harju[1,3], O. Asvany[2], M. Juvela[1,3], and S. Schlemmer[2]

[1] Observatory, PO Box 14, 00014 University of Helsinki, Finland
e-mail: olli.sipila@helsinki.fi
[2] I. Physikalisches Institut, Universität zu Köln, Germany
[3] *Present address*: Department of Physics, PO Box 64, 00014 University of Helsinki, Finland

Received 25 September 2009 / Accepted 5 November 2009

ABSTRACT

Context. The depletion of heavy elements in cold cores of interstellar molecular clouds can lead to a situation where deuterated forms of H_3^+ are the most useful spectroscopic probes of the physical conditions.
Aims. The aim is to predict the observability of the rotational lines of H_2D^+ and D_2H^+ from prestellar cores.
Methods. Recently derived rate coefficients for the $H_3^+ + H_2$ isotopic system were applied to the "complete depletion" reaction scheme to calculate abundance profiles in hydrostatic core models. The ground-state lines of H_2D^+(o) (372 GHz) and D_2H^+(p) (692 GHz) arising from these cores were simulated. The excitation of the rotational levels of these molecules was approximated by using the state-to-state coefficients for collisions with H_2. We also predicted line profiles from cores with a power-law density distribution advocated in some previous studies.
Results. The new rate coefficients introduce some changes to the complete depletion model, but do not alter the general tendencies. One of the modifications with respect to the previous results is the increase of the D_3^+ abundance at the cost of other isotopologues. Furthermore, the present model predicts a lower H_2D^+ (o/p) ratio, and a slightly higher D_2H^+ (p/o) ratio in very cold, dense cores, as compared with previous modelling results. These nuclear spin ratios affect the detectability of the submm lines of H_2D^+(o) and D_2H^+(p). The previously detected H_2D^+ and D_2H^+ lines towards the core I16293E, and the H_2D^+ line observed towards Oph D can be reproduced using the present excitation model and the physical models suggested in the original papers.

Key words. ISM: clouds – radio lines: ISM – astrochemistry – radiative transfer – ISM: abundances – ISM: molecules

1. Introduction

The rate coefficients for reactive and inelastic collisions between the H_3^+ ion and H_2 with all possible deuterated variants and nuclear spin symmetries have been recently derived and a few of them have been experimentally tested by Hugo et al. (2009). Besides making state-specific astrochemical models viable, the cross-sections derived in this work make it possible to model the intensities of the dipole-allowed rotational transitions of H_2D^+ and D_2H^+.

The H_2D^+ and D_2H^+ ions are potentially useful probes of pre-protostellar cores (see e.g. Caselli et al. 2003; Vastel et al. 2004; van der Tak et al. 2005; Pagani et al. 2009). Together with the isotopologues H_3^+ and D_3^+, they are likely to belong to the most abundant ions in the dense and cold nuclei of prestellar cores, where the usual tracer molecules can have practically disappeared from the gas phase (Roberts et al. 2003; Walmsley et al. 2004) – this state of matters is called "complete depletion" in the latter paper. While it has been observed that heavier substances such as CN can exist in the gas phase at densities of the order of 10^6 cm^{-3} (Hily-Blant et al. 2008), the assumption of complete depletion remains a valid first approximation at high densities.

The astrophysical significance of these ions is related to the facts that H_3^+ originates almost directly in the cosmic ray ionization of H_2, and that it initiates the ion-molecule reactions in dense clouds (Herbst & Klemperer 1973). Furthermore, the deuteration of H_3^+ depends on the ortho-para ratio of H_2, which is likely to be non-thermal and evolve with time in interstellar clouds (Pagani et al. 1992; Gerlich et al. 2002; Flower et al. 2006; Pagani et al. 2009).

In this paper we apply the newly derived chemical rate coefficients to the "completely depleted" case first discussed by Walmsley et al. (2004), and use the state-to-state coefficients to predict the ground-state rotational lines of *ortho*-H_2D^+ and *para*-D_2H^+ from prestellar cores. The two core models used in these simulations correspond to the observed properties of the cores Oph D and I16293E in Ophiuchus. The rate coefficients of Hugo et al. (2009) for some important deuteration reactions differ from those adopted in Roberts et al. (2003), and in the series of papers by Flower, Pineau des Forêts & Walmsley, and we discuss changes implied to the complete depletion model. The Hugo et al. (2009) rate coefficients have been previously used by Pagani et al. (2009) in the modelling of the prestellar core L183, where also CO, N_2 and their derivatives were included in the chemical reaction scheme. The organization of the present paper is as follows: in Sect. 2, we describe the physical and chemical models and, in Sect. 3, we present the modelling results. The results are discussed in Sect. 4, and finally, the main points of this discussion are summed up in Sect. 5.

2. Model

In what follows, we describe the model assumptions. These include the physical core model, the description of the dust grain component, the chemical reaction scheme, and the adopted rate coefficients. We also give a brief account of the methods and programs used in solving the chemical abundances and the emitted molecular line radiation.

2.1. Core model

For the core model we used a modified Bonnor-Ebert sphere (BES), which is a non-isothermal cloud in hydrostatic equilibrium (previously discussed by, e.g., Evans et al. 2001), heated externally by the interstellar radiation field, ISRF. The possibility of a hydrostatic or near-equilibrium configuration is suggested by observations towards some prestellar cores which seem to represent an advanced stage of chemical evolution (characterized by a high degree of molecular depletion), and have near-thermal linewidths (e.g., Bergin & Tafalla 2007).

We first calculated a density profile resulting from an isothermal model (Bonnor 1956). The density profile was then fed into a Monte Carlo radiative transfer program (Juvela & Padoan 2003; Juvela 2005) for the temperature calculation. For this purpose the core model was divided into concentric shells. We used the grain size distribution of Mathis et al. (1977) (MRN) with two types of dust grains: carbonaceous and silicate (the grain model is further discussed in Sect. 2.2.4). The choice of using the MRN distribution implies that the abundance of very small grains (with radii less than ~0.01 μm) is assumed to be negligible, and that grain coagulation is not considered. The temperature profile was calculated separately for the two dust types. In each position of the core, the final temperature profile was taken to be the arithmetic average of the temperatures of both grain types.

The gas and dust temperatures were assumed to be equal. While this is probably a good approximation in the dense ($>10^6$ cm^{-3}) central part of the core (Burke & Hollenbach 1983), it may not hold as well in the outer layers of the core (~10^5 cm^{-3}, Bergin et al. 2006). In the present analysis, which concentrates on the very dense nucleus of the core, we have ignored this phenomenon. The model core is assumed to be embedded in a molecular cloud with extinction corresponding to $A_V = 10^m$. This assumption agrees with observations from the vicinity of Oph D (Chapman et al. 2009).

To determine the exact core density profile using the computed temperature distribution, we slightly modified the method used in Bonnor (1956) by making the following substitutions:

$$\rho = \lambda \left(\frac{T_c}{T}\right) e^{-\psi} \tag{1}$$

$$r = \beta^{1/2} \lambda^{-1/2} \xi, \tag{2}$$

where $\beta = k_B T_c / 4\pi G m$, T_c is the temperature in the center of the core and m is the mass of the hydrogen molecule. As in Bonnor (1956), λ was chosen to be the central density. We also imposed the boundary conditions $\psi = 0$, $d\psi/d\xi = 0$ and $dT/d\xi = 0$ in the centre of the core. Substituting the above expressions into the equation of hydrostatic equilibrium (Bonnor's Eq. (2.2)) and keeping in mind that $T = T(r)$, one obtains

$$\frac{d^2\psi}{d\xi^2} = \left(\frac{T_c}{T}\right)^2 e^{-\psi} - \frac{2}{\xi}\frac{d\psi}{d\xi} - \frac{1}{T}\frac{dT}{d\xi}\frac{d\psi}{d\xi}. \tag{3}$$

Equation (3) was integrated numerically and the resulting density profile was fed back into the radiative transfer program to calculate a new temperature profile. This procedure was repeated a few times until the density profile converged.

2.2. Chemistry model

We adopted the complete depletion model discussed in Walmsley et al. (2004) and Flower et al. (2004). The reaction scheme is fairly simple: the gas-phase reactants include only H, H^+, H_2, H_2^+, H_3^+ and their deuterated forms, He, He^+, and free electrons. Because of the low temperature associated with the environment, the zero-point energies become relevant and thus the deuterated forms and different nuclear spin modifications have to be considered explicitly. The reaction set also includes cosmic ray ionization, H_2 formation on grains, and some other grain processes. We next discuss the gas-phase and grain-surface reactions separately.

2.2.1. Gas phase chemical reactions

In all our models, we assumed that the core is electrically neutral, i.e. that electron abundance equals the difference between the total abundance of positive ions and the abundance of negatively charged grains.

The chemical reactions and the associated rate coefficients were compiled using four sources: Walmsley et al. (2004), Flower et al. (2004), Hugo et al. (2009), and Pagani et al. (2009). The reaction set of Walmsley et al. (2004) was complemented by Flower et al. (2004) to include the nuclear spin modifications of D_2, D_2H^+, and D_3^+. Hugo et al. (2009) took the analysis of the $H_3^+ + H_2$ reacting system further by using a microcanonical approach to derive state-to-state rate coefficients. This approach differs from that of Flower et al. (2004) in that all internal states of the reacting system are explicitly taken into account, resulting in detailed state-to-state rate coefficients for different configurations of the system. We adopted their ground state-to-species rate coefficients for all reactions relevant to the $H_3^+ + H_2$ system (including the deuterated forms) and substituted them into the combined data of Walmsley et al. (2004) and Flower et al. (2004). Furthermore, for dissociative recombination (DR) reactions of H_3^+ and its deuterated forms we used the newly calculated rate coefficients presented in Appendix B of Pagani et al. (2009).

2.2.2. Grain reactions

The H_2 and HD molecules are mainly formed on grain surfaces (Gould & Salpeter 1963; Hollenbach & Salpeter 1971), whereas for the formation of D_2, gas-phase reactions are more important. Nevertheless, the formation of all three isotopologues on dust grains, and the corresponding destruction terms for atomic H and D were included in the chemical system. We assumed that *ortho* and *para* forms are produced according to their statistical population ratios 3:1 and 2:1 for H_2 and D_2, respectively.

Grain processes, in particular the formation of *ortho*-H_2 and the attachment and destruction of positive ions on grain surfaces, are important for the overall degree of deuteration of the cloud (see Sect. 4). The details of these processes (grain surface properties, desorption mechanisms, etc.) were not considered in the present model. It was assumed that chemical reactions on grains (along with the associated adsorption and desorption) take place instantaneously.

The rate coefficients for grain reactions (including, e.g., electron attachment and recombination of positive ions on grains), listed in Walmsley et al. (2004), were taken from Flower & Pineau des Forêts (2003), in which an MRN distribution with $a_{min} = 0.01$ μm, $a_{max} = 0.3$ μm was assumed. These limits correspond to an effective grain radius of $a_{eff} = 0.0202$ μm[1]. Since the rate coefficient for a grain reaction is proportional to $\sigma_g = \pi a_{eff}^2$,

[1] The rate coefficients of grain reactions listed in Table A.1. of Walmsley et al. (2004) correspond to $a_{eff} = 0.02$ μm, contrary to what is said in the caption.

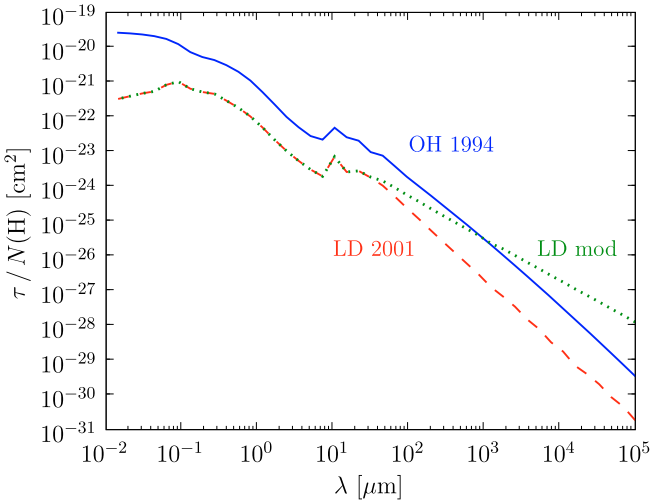

Fig. 1. Optical thickness per column density according to the opacity data of Ossenkopf & Henning (1994), denoted in the figure by "OH 1994", (solid curve) and Li & Draine (2001), denoted by "LD 2001" (dashed curve). The modified extinction curve (see text) is also plotted, denoted by "LD mod" (dotted curve).

we scaled the Flower & Pineau des Forêts (2003) coefficients by $(a_{\rm eff}/0.02\,\mu{\rm m})^2$, where $a_{\rm eff}$ is the effective grain radius of the assumed size distribution. The Coulomb factor, $\tilde{J}(\tau, \nu)$, which takes into account the electric interaction between dust grains and gas phase neutrals and/or ions, was included as an additional factor. Its mathematical form has been discussed in detail in Draine & Sutin (1987), and recently in Pagani et al. (2009).

2.2.3. Molecular line radiation

The abundance distributions of chemical species were determined by a chemistry program in physical conditions corresponding to those in different parts of the model core – in practice in each of the concentric shells used in the temperature calculations. The radial H_2D^+(o) and D_2H^+(p) abundance distributions, together with the density and temperature profiles were used as input for a Monte Carlo radiative transfer program (Juvela 1997) to predict observable line emission.

The excitation of the rotational transitions of H_2D^+(o) and D_2H^+(p) in collisions with *para* and *ortho* H_2 were calculated using the state-to-state rate coefficients from Hugo et al. (2009). The data concerning the line frequencies and Einstein A coefficients were obtained from Miller et al. (1989), Ramanlal & Tennyson (2004), and Amano & Hirao (2005).

2.2.4. Dust grain model

The MRN model was adopted for the grain size distribution. In the density and temperature profile calculations, we used two types of grains; carbonaceous and silicate. The optical properties of these components were adopted from Li & Draine (2001). The densities of the carbonaceous and silicate grains were taken to be 2.5 g cm^{-3} and 3.5 g cm^{-3}, respectively. In the chemistry model, no separation between the grain materials was done, and a grain material density of 3.0 g cm^{-3} was assumed. For the comparison with the Flower et al. (2004) results (Sect. 3.1) we used, however, the same assumptions of the grain material density (2.0 g cm^{-3}) and dust-to-gas mass ratio (0.013) as in Walmsley et al. (2004).

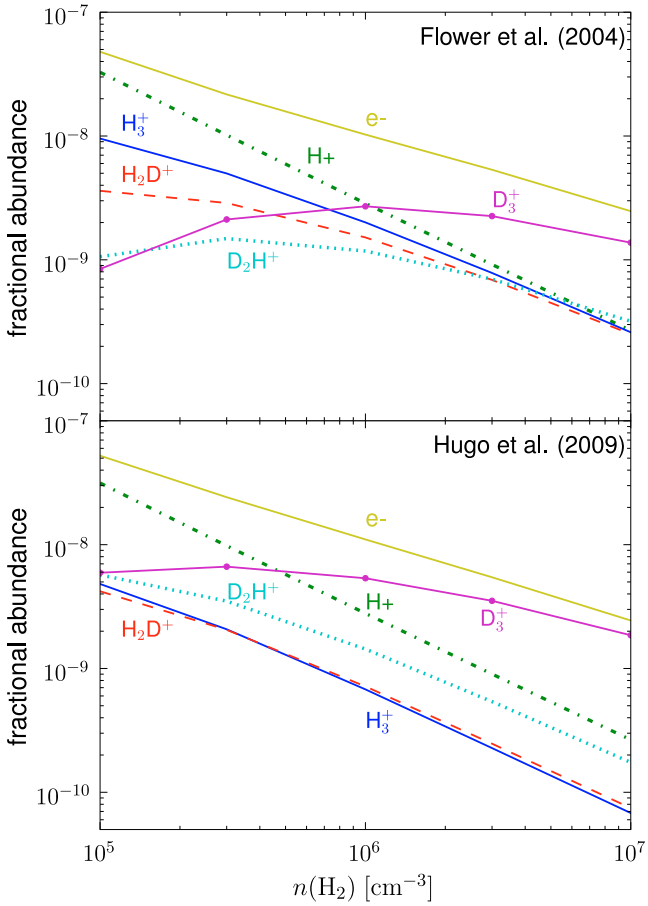

Fig. 2. Steady state abundances of electrons, protons, H_3^+ and its deuterated forms, calculated using the Flower et al. (2004) (*upper panel*) and Hugo et al. (2009) (*lower panel*) rate coefficients in an isothermal (T = 10 K) model with single size grains (a = 0.1 μm). A cosmic ray ionization rate of $\zeta = 3 \times 10^{-17}$ s^{-1} is assumed.

The model of Li & Draine (2001) describes dust in diffuse medium. In dense clouds, coagulation and growth of icy grain mantles are expected to modify the grain properties and, according to the models of Ossenkopf & Henning (1994), the extinction curve is expected to become flatter in the far-infrared and at longer wavelengths. Since in our cores the central densities are high, $n(\mathrm{H}) \sim 10^6$ cm^{-3}, we modified the Li & Draine (2001) dust opacities accordingly. This leads to temperatures of the order of 6 K in the core center. The curves are plotted in Fig. 1.

3. Results

In this Section we discuss the differences arising from the use of the modified chemical reaction rate coefficients used in this paper compared to those used in Flower et al. (2004). We then present results of chemical modelling carried out using a hydrostatic core model. We conclude the section with a brief discussion on simulated line emission spectra.

3.1. Comparison with Flower et al. (2004) results using homogeneous models

We ran a set of homogeneous models corresponding to those presented in Walmsley et al. (2004) and in Flower et al. (2004). The steady state fractional abundances of the principal ions as

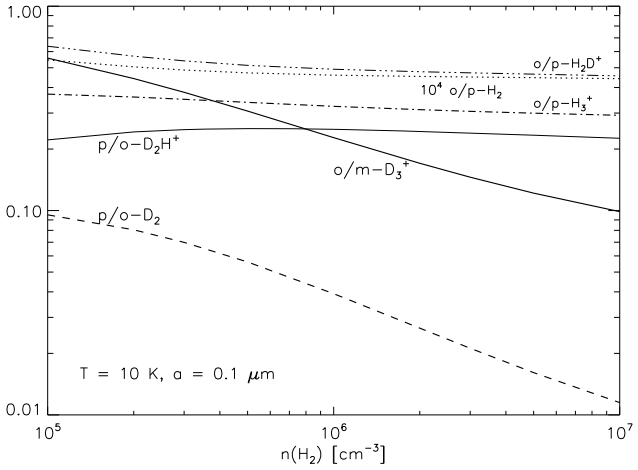

Fig. 3. Steady-state abundance ratios of the nuclear spin modifications of H_2, D_2, H_3^+ and its deuterated forms as functions of $n(H_2)$ calculated using Hugo et al. (2009) rate coefficients. The model parameters are the same as used in Fig. 2.

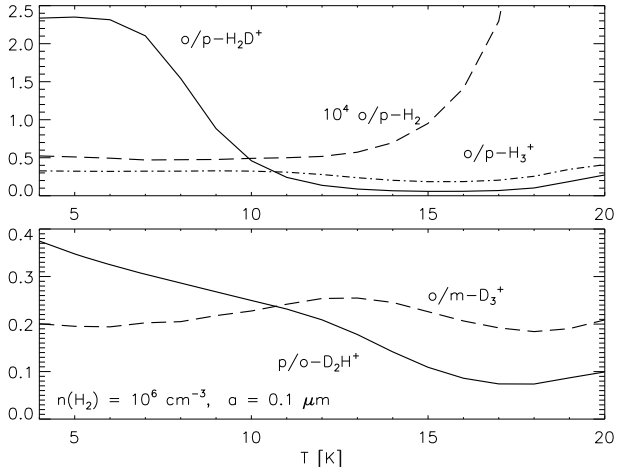

Fig. 4. Steady-state o/p ratios of H_2 (multiplied by 10^4), H_3^+, and H_2D^+ (*top panel*), and the steady-state D_2H^+ (p/o) and D_3^+ (m/o) ratios (*bottom panel*) as functions of the gas temperature in the range 4–20 K. The assumed gas density and grain radius are $n(H_2) = 10^6$ cm^{-3} and $a = 0.1\,\mu$m, respectively.

functions of the gas density are shown in Fig. 2. The upper diagram corresponds to the Flower et al. (2004) model and is a reproduction of their Fig. 1. The lower plot is produced using the Hugo et al. (2009) rate coefficients for the $H_3^+ + H_2$ isotopic system and the DR rate coefficients from Pagani et al. (2009). The figures were produced assuming an isothermal ($T = 10$ K) model with single sized grains ($a = 0.1\,\mu$m) and a grain material density of 2.0 g cm^{-3}.

The abundance ratios of the most important nuclear spin variants as functions of the gas density are shown in Fig. 3, and the temperature dependence at low temperatures is illustrated in Fig. 4. The former should be compared with Fig. 2 of Flower et al. (2004) and with Fig. 3 of Walmsley et al. (2004), and the latter with Figs. 5 and 6 in Flower et al. (2004). Following Hugo et al. (2009) we have assigned *meta*-D_3^+ with the modification having the lowest ground state energy, corresponding to the A_1 representation of the symmetry group S_3, and *ortho*-D_3^+ with the E representation (see their Sect. II.A.1). The *ortho* and *meta* appelations for D_3^+ are therefore interchanged with respect to those used in Flower et al. (2004), Pagani et al. (2009), and most other papers. As in Flower et al. (2004), the D_3^+ (o/m) and D_2 (p/o) ratios fall rapidly with increasing $n(H_2)$. However, the D_2H^+ (p/o) ratio is nearly constant unlike in the previous study. The H_3^+ (o/p) ratio is about three times lower in the present model. There are also a couple of differences in the temperature dependence (Fig. 4). The H_2D^+ (o/p) ratio levels off between 2–3 when approaching very low temperatures. Using the Flower et al. (2004) rate coefficients the corresponding value is ∼10 in the same conditions. Secondly, the D_2H^+ (p/o) reaches slightly higher (0.3–0.4) at very low temperatures than in the Flower et al. (2004) model. We note that as our model follows the chemistry until steady state, the H_2 (o/p) ratio becomes much lower than in the models of Pagani et al. (2009). As a consequence, we obtain a clearly higher degree of deuteration of H_3^+ and somewhat different nuclear spin ratios for its isotopologues as compared with this previous study. We return to this matter briefly in Sect. 4.1.

All the plots presented so far assume single sized grains with a radius of 0.1 μm. As discussed in Sect. 3.3 of Flower et al. (2004), the grain size has a considerable effect on the abundances and nuclear spin ratios. The D_2 (o/p), D_2H^+ (o/p), and D_3^+ (m/o) ratios peak near the grain radius $a = 0.1\,\mu$m (see Fig. 9 in Flower et al. 2004), whereas the H_2 (o/p), H_3^+ (o/p), and H_2D^+ (o/p) ratios increase monotonically towards smaller grain radii.

3.2. Hydrostatic models

We studied the influence of the grain size distribution and the cosmic ionization rate on the chemistry of a depleted, hydrostatic core. The model BE sphere was assumed to have a central density of $n(H_2) = 2 \times 10^6$ cm^{-3} and an outer radius of 2400 AU, where the density drops to about 10^5 cm^{-3}. These parameters correspond roughly to the dense nucleus of the Oph D core according to Harju et al. (2008). The effective grain radius was varied by changing the lower limit of the grain size distribution and keeping the upper limit constant at 0.3 μm. Modelling was carried out with effective grain radii of 0.05 μm, 0.1 μm and 0.2 μm. The slope of the extinction curve (Fig. 1) was modified to produce a central core temperature of about 6 K (see Sect. 2.2.4). The chemical reaction network was integrated until $t = 2 \times 10^6$ years, which was well within steady state (all the abundances settled into steady state at times $<10^6$ years).

Figure 5 shows the core density profile corresponding to effective grain radius $a_{\rm eff} = 0.1\,\mu$m. The temperature profiles for three different grain sizes are superposed. Changing $a_{\rm eff}$ has a marked effect on the temperature profile, but alters the density distribution only slightly (the central density is kept fixed in our models). The core gets colder as the effective grain radius gets smaller; this is because the total grain surface area (effectively the total opacity) grows larger as the effective grain radius decreases.

Figure 6 shows the steady state fractional abundance profiles of the principal ions for the selected values of effective grain radius and for a cosmic ray ionization rate of $\zeta = 3 \times 10^{-17}$ s^{-1}. The grain radius decreases from top to bottom. As shown in Fig. 5, this decrease is accompanied by a slight drop in the average temperature. The fractional ion abundances generally decrease towards the core centre, i.e., towards higher densities, in accordance with the results from homogeneous models shown in Fig. 2. The density dependence of D_3^+ is less marked, which leads to an increased degree of deuterium fractionation in the centre when the effective grain radius decreases. The fractional H^+ abundance decreases drastically with decreasing grain

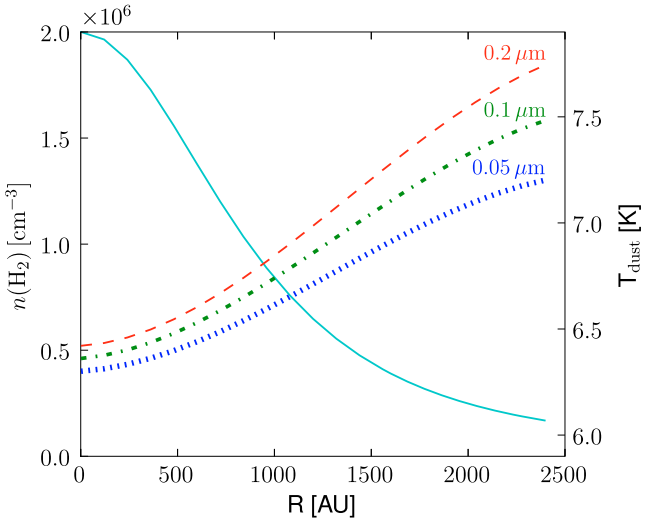

Fig. 5. The radial core density profile corresponding to effective grain radius $a_{\rm eff} = 0.1$ μm, with a central temperature of ∼6.4 K. Radial temperature profiles corresponding to different values of effective grain radius (indicated in the figure) are superposed.

size. This is caused by accentuated recombinations on negatively charged grains as explained in Walmsley et al. (2004).

The radial profiles of the H_2 (o/p), H_3^+ (o/p), H_2D^+ (o/p), D_2H^+ (p/o), and D_3^+ (o/m) ratios are presented Fig. 7. While most ratios have rather flat distributions, the D_3^+ (o/m) ratio drops towards the centre, i.e. towards higher densities. The density dependence is, however, smoother for small grain sizes (bottom panel). The ortho/para ratios of H_2, H_3^+, and H_2D^+ increase from top to bottom, along with the decreasing grain size. This is caused by an intensified replenishment of H_2(o) when the total grain surface area becomes larger. The slight increase of H_2 (o/p) towards the outer parts reflects the decreasing density (see Fig. 3). The H_3^+ (o/p) ratio follows the H_2 (o/p) ratio closely. The H_2D^+ (o/p) ratio correlates with the H_2 (o/p) ratio, but rises towards low temperatures (see Fig. 4). These tendencies result in a slight increase of the H_2D^+ (o/p) ratio towards the core centre. The D_2H^+ (p/o) ratio changes very little as a function of radius and from model to model. Like the D_3^+ (o/m) ratio, the D_2H^+ (o/p) ratio has a flat maximum around $a \sim 0.1$ μm (Flower et al. 2004), and depends weakly on the density (Fig. 3).

The effect of changes in the cosmic ionization rate, ζ, is illustrated in Fig. 8. This shows the radial distributions of the principal ions for the cases where ζ is made 10 times lower (top) and 10 times higher (bottom) than in the models discussed above. Lowering ζ decreases the degree of ionization. An enhanced cosmic ray ionization increases the ion abundances, but decreases the deuteration through an intensified electron recombination (Walmsley et al. 2004; Flower et al. 2004). The effect is particularly marked for D_3^+ near the outer edge of the core.

3.3. H_2D^+ and D_2H^+ spectra

We calculated the spectral line profiles of the ground state transitions of H_2D^+(o) (1_{10}–1_{11}, 372 GHz) and D_2H^+(p) (1_{10}–1_{01}, 692 GHz) from models corresponding to the observed properties of the prestellar cores I16293E and Oph D.

The very narrow 372 GHz line of H_2D^+(o) detected with APEX towards the density maximum of Oph D has been suggested to originate in a hydrostatic core (Harju et al. 2008). In

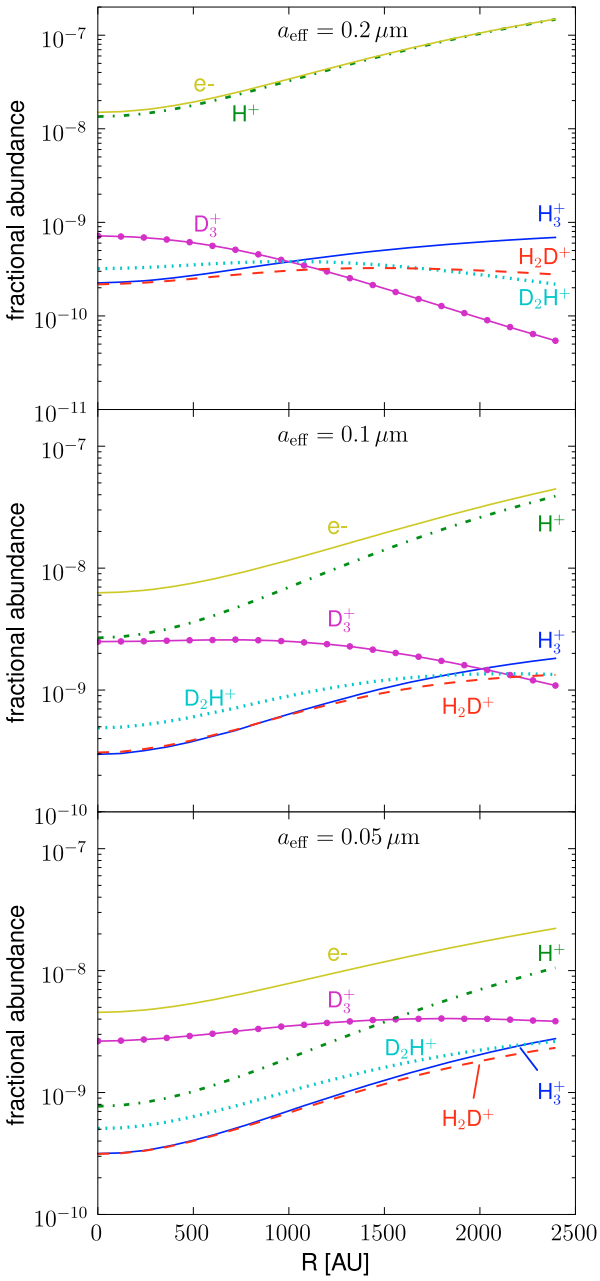

Fig. 6. Radial fractional (with respect to $n(H_2)$) adundance profiles of electrons, H^+, H_3^+ and its deuterated forms at $t = 1 \times 10^6$ years, for a cosmic ray ionization rate $\zeta = 3 \times 10^{-17}$ s^{-1}.

accordance with this suggestion the physical model used for Oph D is a hydrostatic core heated externally by the interstellar radiation field (ISRF). Judging from previous maps, in particular the ISOCAM 7 μm image from Bacmann et al. (2000), we assumed an angular radius of 20″. We adopted the recent distance estimate of 120 pc to the Ophiuchus complex (Lombardi et al. 2008), which implies that the adopted radius corresponds to 2400 AU. The obscuration provided by the surrounding molecular cloud was assumed to correspond to $A_{\rm V} = 10^{\rm m}$. We varied the central H_2 density (n_0), the effective grain radius ($a_{\rm eff}$), and the cosmic ray ionization rate (ζ), and calculated the appropriate abundance profiles using the chemistry model described above. Finally, the populations of the rotational levels of H_2D^+(o), and

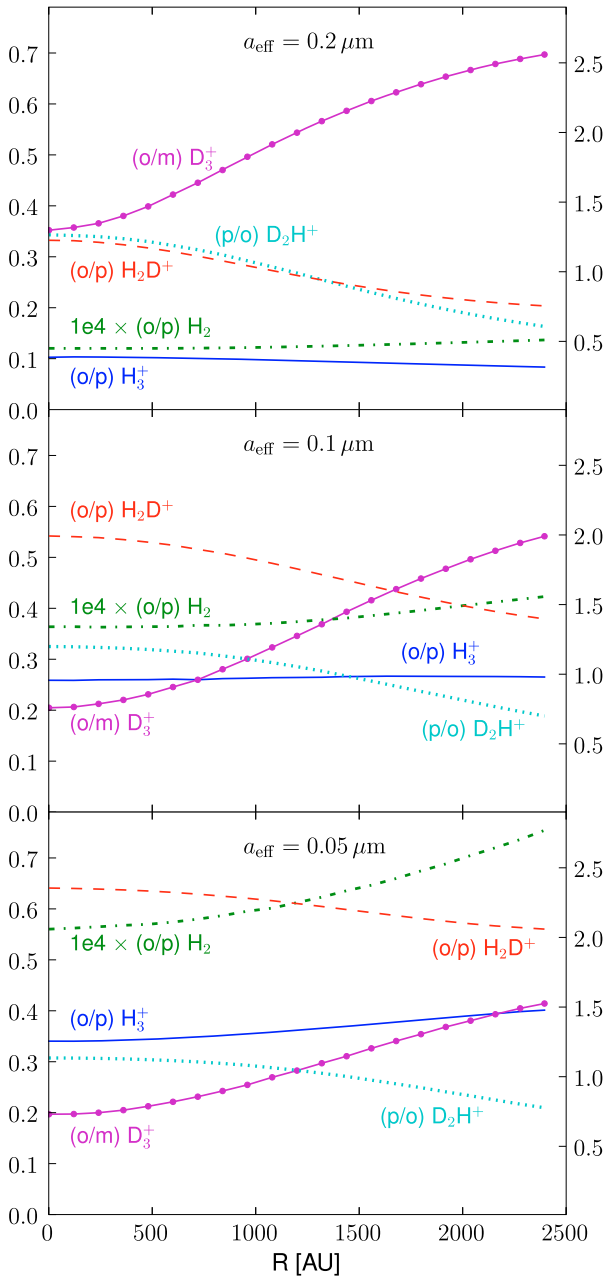

Fig. 7. Radial profiles for the ratios of the different spin states of H_2, H_3^+ and its deuterated forms at $t = 1\times10^6$ years, for a cosmic ray ionization rate $\zeta = 3 \times 10^{-17}$ s^{-1}. The y-axis on the right side denotes the H_2D^+ (o/p) ratio.

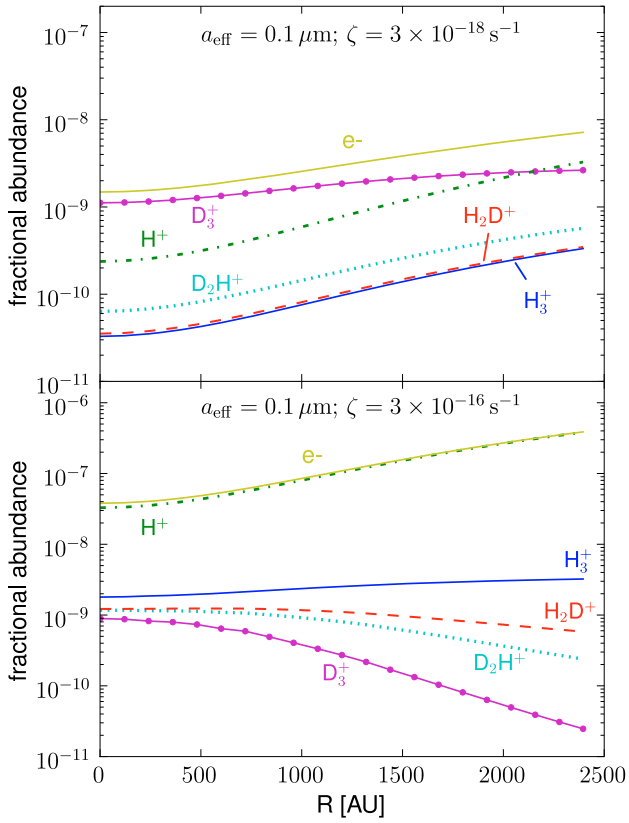

Fig. 8. Same as the middle panel in Fig. 6, but for cosmic ray ionization rates $\zeta = 3\times10^{-18}$ s^{-1} (*upper panel*) and $\zeta = 3\times10^{-16}$ s^{-1} (*lower panel*).

the $1_{10} - 1_{11}$ line profiles were calculated using the state-to-state rate coefficients for H_2D^+(o) + H_2 (para and ortho separately) collisions from Hugo et al. (2009) and our Monte Carlo radiative transfer program. Calculations with different values for the model parameters were carried out until a reasonable agreement with the observed H_2D^+(o) profile was met. This model was then used to predict the D_2H^+(p) line at 692 GHz as observed with APEX.

The results of our simulations are presented in Fig. 10, which also shows the observed H_2D^+(o) spectrum. The best fit was obtained using the following parameters: $n_0 = 2 \times 10^6$ cm^{-3}, $a_{\rm eff} = 0.1\,\mu$m, and $\zeta = 6 \times 10^{-17}$ s^{-1}. The model core has a central temperature $T = 6.36$ K. The fractional H_2D^+(o) abundance is $\sim3.6 \times 10^{-10}$ in the core center, rising to $\sim7.2 \times 10^{-10}$ at the edge. A Gaussian fit to the model spectrum yields an *FWHM* of 0.35 km s^{-1}; the peak optical depth is $\tau_{\rm peak} \sim 1.5$. A molecular line profile for the D_2H^+(p) 1_{10}–1_{01} transition using the same core model parameters is shown in the lower panel of the figure. A Gaussian fit to the spectrum yields an *FWHM* of 0.27 km s^{-1}, the peak optical depth is $\tau_{\rm peak} \sim 0.6$. The D_2H^+(p) abundance is $\sim1.4 \times 10^{-10}$ at the core center and $\sim1.1 \times 10^{-10}$ at the edge – essentially a flat profile with a minor maximum at around 1200 AU.

Both H_2D^+ and D_2H^+ have been detected with the CSO towards I16293E by Vastel et al. (2004). To our knowledge this work has produced the only rather firm detection of the 692 GHz line so far. Vastel et al. (2004) estimated the H_2D^+(o) and D_2H^+(p) column densities from the observed line profiles by assuming line-of-sight homogeneity and an excitation temperature of $T_{\rm ex} = 10$ K. We assumed that these column densities are approximately valid, and adjusted the fractional abundances accordingly. The physical model of the core was adopted from Stark et al. (2004), allowing for the fact that the cloud is probably nearer than previously thought (120 pc, Lombardi et al. 2008). The model consisted of a compact, homogeneous nucleus with a density $n_0 = 1.6 \times 10^6$ cm^{-3} up to a radius of 750 AU, surrounded by an envelope with the density power law $n \propto r^{-1}$ extending to a distance of 6000 AU (50″). A dust temperature $T_{\rm dust} = 16$ K derived by Stark et al. (2004) was adopted as the temperature of the nucleus. The dust temperature was gradually increased toward the core edge, reaching a value $T_{\rm dust} = 20$ K at 6000 AU. It should be noted, however, that the observations of Vastel et al. (2004) suggest a lower value for the region where the

H_2D^+ and D_2H^+ emission originate. Assuming thermal broadening only, the line widths listed in their Table 1 imply kinetic temperatures $T_{\rm kin} = 11.2 \pm 2.5$ (H_2D^+) and $T_{\rm kin} = 9.1 \pm 4.4$ (D_2H^+). These estimates are upper limits as they neglect the possible turbulent broadening and instrumental effects. In order to reproduce the column densities derived by Vastel et al. (2004), the fractional H_2D^+(o) abundance was set to $\sim 10^{-10}$ in the nucleus, and it was let to fall radially to $\sim 10^{-11}$ at the outer edge. The D_2H^+(p) abundance was set at 0.6 times the H_2D^+(o) abundance, which is within the column density error range reported by Vastel et al. (2004).

The line profiles calculated from this model are shown in Fig. 11. The simulated H_2D^+(o) line has a peak optical depth $\tau \sim 0.33$. A Gaussian fit to the spectrum yields an *FWHM* of ~ 0.46 km s^{-1} and a peak antenna temperature $T_{\rm A}^* \sim 1.42$ K. The simulated D_2H^+(p) line yields $\tau \sim 0.30$, an *FWHM* of ~ 0.41 km s^{-1} and a peak $T_{\rm A}^* \sim 0.44$ K. The antenna temperatures of the simulated H_2D^+(o) and D_2H^+(p) spectra agree well with the observations of Vastel et al. (2004), but the lines are too broad, probably because the assumed kinetic temperature is too high. We return to this issue in Sect. 4.3.

4. Discussion

We now discuss in more detail the results presented in the last section, starting with the differences in homogeneous models arising from using different rate coefficients. We then discuss the abundance distributions in our hydrostatic core models, and conclude by looking into the simulated line emission spectra.

4.1. Homogeneous models

In the models calculated using the new reaction rate coefficients derived by Hugo et al. (2009), the deuteration of H_3^+ proceeds faster than in the models of Flower et al. (2004). As a consequence, D_3^+ becomes the dominant ion at relatively low densities. The total[2] rate coefficients of Hugo et al. (2009) for the deuteration reactions $H_3^+ \rightarrow H_2D^+ \rightarrow D_2H^+ \rightarrow D_3^+$ are larger than those used by Flower et al. (2004) by an average factor of ~4–5. This difference originates in the discrepancy between the laboratory measurements of Gerlich et al. (2002) and Hugo et al. (2009, see their Sect. IV.C) concerning the forward rate coefficients at very low temperatures. On the other hand, the total rate coefficients for the "backward" reactions (k_{-1}, k_{-2}, k_{-3}) are similar in the two reaction schemes. This can be traced to the fact that the "backward" rate coefficient for the reaction H_2D^+(o) + H_2(o) $\stackrel{k_{-1}(\rm oo)}{\longrightarrow}$ H_3^+(o/p) + HD derived by Hugo et al. (2009) agrees with the estimate of Gerlich et al. (2002, Sect. 3.3).

The ratios $K = k/k_-$ are thus larger in Hugo et al. (2009) which implies that chemical equilibrium is established at higher concentrations of deuterated species. The equilibrium constants in the present model are, however, smaller than in the models of Roberts et al. (2004) and Caselli et al. (2008). The forward rate coefficients of Hugo et al. (2009) are similar to those used in the two previous studies while the backward rate coefficents are several orders of magnitude larger owing to the non-thermal H_2 (o/p) ratio.

As discussed in Flower et al. (2006), the *ortho*/*para* ratios of H_3^+ and H_2D^+ correlate with H_2(o/p) through proton exchange reactions. The H_3^+ ion is primarily produced in the *para* form via the reaction of H_2^+(p) with H_2(p). The *para-ortho* and *ortho-para* conversions through reactions with H_2(o) are, however, rapid, and compete only against the deuteration reaction with HD. In the conditions considered here a good approximation of the o/p ratio can be obtained from

$$\mathrm{H_3^+(o/p)} \approx \frac{k_{\rm po}\,\mathrm{H_2(o/p)}}{k_{1\rm o}\,x(\mathrm{HD}) + k_{\rm op}\,\mathrm{H_2(o/p)}},$$

where $k_{\rm po}$ and $k_{\rm op}$ are the rate coefficients of the nuclear spin changing reactions of H_3^+(p) and H_3^+(o) with H_2(o) (reactions 6 and 7 in Flower et al. 2006), and $k_{1\rm o}$ is the rate coefficient of the reaction of H_3^+(o) with HD which produces mainly H_2D^+(o) (see Table VIII in Hugo et al. 2009). Using the Hugo et al. (2009) rate coefficients, with $k_{\rm po} \sim k_{\rm op} \sim 0.3k_{1\rm o}$, we obtain a steady-state ratio of H_3^+(o/p) ~ 0.2–0.4 in cold, dense gas, where H_2(o/p) ~ x(HD) (see Fig. 4).

Also for H_2D^+, the nuclear spin changing reactions with H_2 are effective and an approximate value of the o/p ratio can be obtained through balancing these according to Eq. (7) of Gerlich et al. (2002). Below ~8 K, however, primary production from H_3^+ + HD and destruction through the secondary deuteration reaction $H_2D^+ + HD \rightarrow D_2H^+ + H_2$ start to dominate. At very low temperatures the H_2D^+ (o/p) ratio settles somewhere between 2 and 3 (Fig. 4).

The production and destruction of *ortho* and *para* D_2H^+ occur mainly via the deuteration reactions $H_2D^+ + HD \rightarrow D_2H^+ + H_2$ and $D_2H^+ + HD \rightarrow D_3^+ + H_2$. As discussed in Flower et al. (2006), the lower energy *ortho* state is favoured in the reverse reactions with H_2(o) (reactions 11 and 12 in their Sect. 3.4; Table VIII in Hugo et al. 2009). Moreover, D_2H^+(p) is reduced through *para-ortho* conversion in the reaction with HD. In the present model the p/o ratio is ~0.2–0.4 below 10 K and is not sensitive to $n(H_2)$.

We note that while the H_2D^+ (o/p) ratio is similar to that found in the models of Pagani et al. (2009, Fig. 9), the D_2H^+ (p/o) ratio is larger by a factor of 2–4 in the present model. By performing some test runs we could establish that the main reason for this apparent discrepancy is in the different H_2 (o/p) ratio. In the time-dependent model of Pagani et al. (2009), the initial H_2 (o/p) ratio is larger than unity, and the chemical evolution is followed until the model matches with the constraints based on observations of the N_2D^+/N_2H^+ ratio toward the L183 core. The resulting H_2 (o/p) ratio (~0.005–0.05) is much higher than in our models (less than 10^{-4}). At a high H_2 (o/p) ratio, D_2H^+(p) is mainly destroyed in the reaction D_2H^+(p) + H_2(o) → H_2D^+(p) + HD, and the destruction by HD (including para-ortho conversion) is not significant.

The principal reactions determining the *ortho*/*meta* ratio of D_3^+ are discussed in Flower et al. (2004) (Appendix B, with interchanged *meta* and *ortho* appellations with respect to the present work). The (lowest energy) *meta* form of D_3^+ is primarily formed via deuteration of D_2H^+(o) by HD, and via *ortho-meta* conversion in reaction D_3^+(o) + HD → D_3^+(m) + HD. The destruction of D_3^+(m) is overwhelmingly dominated by dissociative recombination with electrons or negatively charged grains. For D_3^+(o),

[2] By the "total rate coefficients" we mean the resultant forward and backward rate coefficients, k_1 and k_{-1}, in the presentation omitting the nuclear spin variants, e.g., $H_3^+ + HD \underset{k_{-1}}{\overset{k_1}{\rightleftharpoons}} H_2D^+ + H_2$. In this presentation, the H_2D^+ formation rate can be written $k_1[H_3^+][HD]$, where k_1 is a combination of seven individual rate coefficients weighted according to the fractions of H_3^+(o) or H_3^+(p) of the total H_3^+ abundance (see Table VIII of Hugo et al. 2009). The other deuteration reactions and their reverse reactions are composed of eight reactions. Besides the temperature, the total rate coefficients and the equilibrium constant, $K = k/k_-$, depend on the relative populations of nuclear spin variants, in particular o/p H_2 (e.g. Gerlich et al. 2002).

the reaction $D_2H^+ + HD \rightarrow D_3^+ + H_2$ in the backward direction and the *ortho-meta* conversion mentioned above are comparable with electron recombination as destruction mechanisms. The formula presented in the appendix of Flower et al. (2004) approximates the equilibrium o/m ratio with a high accuracy. The ratio is proportional to the electron density, and decreases as the gas density increases. On the other hand, it changes very little as a function of temperature in the range considered here (see Figs. 3 and 4).

Finally, we note that the D_2 (p/o) ratio correlates with the D_3^+ (o/m) ratio (see Fig. 3). The higher energy D_2(p) is principally formed from D_3^+(o) via dissociative recombination with free electrons and on dust grains, whereas D_2(o) forms primarily from D_3^+(m) (DR rate coefficients from Pagani et al. (2009) and branching ratios from Flower et al. (2004) have been used here). The destruction of D_2(p) is dominated by deuterium exchange reactions with D_3^+(m) and deuteration of H_3^+(p), while for D_2(o) the deuteration of D_2H^+(o) and H_3^+(p) are the most important destruction reactions. The resulting equilibrium D_2 (p/o) ratio is roughly an order of magnitude lower than the D_3^+ (o/m) ratio.

4.2. Hydrostatic models

In the hydrostatic models (Figs. 6 and 7) combined effects of changing grain size, density and temperature can be seen. The decrease of the average grain size from the top panel to the bottom signifies an increase in the total grain surface area. This results in a diminishing fractional abundance of free electrons and a growing abundance of negatively charged grains (owing to the sticking of electrons onto neutral grains), and an increase of the H_2 (o/p) ratio (because of enhanced H_2 formation on grain surfaces). The radial fall off of the density (from left to right) is accompanied by an elevated temperature at the outer edge of the core.

The D_3^+ ion is the most abundant deuterated form of H_3^+ in the centre of the core. In the following we use the D_3^+/H_3^+ abundance ratio to quantify the degree of deuteration. The D_3^+/H_3^+ ratio changes as a function of grain size. For the largest grain size, $a = 0.2\,\mu$m, $[D_3^+]/[H_3^+]$ is ~3.3 in the core center, and ~0.08 at the edge. As the grain size is decreased to $a = 0.1\,\mu$m, $[D_3^+]/[H_3^+]$ increases both in the center (to ~8.6) and at the edge (to ~0.6). For still smaller grains, $a = 0.05\,\mu$m, $[D_3^+]/[H_3^+]$ drops slightly (to 8.5) in the center, but increases to ~1.4 at the edge.

The changes in the deuterium fractionation as functions of the density and the effective grain radius are plotted in Fig. 9 for isothermal models with $T_{\rm kin} = 7$ K. One can see in the plot that for each value of density, there is a deuteration maximum which shifts to lower values of a as the density is decreased. The sloping down of $[D_3^+]/[H_3^+]$ on the right, towards larger grains, is caused by an increasing abundance of free electrons. The decrease of $[D_3^+]/[H_3^+]$ on the left side, towards smaller grains, is caused by the increase in the abundance of H_2(o) which hinders deuteration by converting H_2D^+ back to H_3^+, and by the increase of negatively charged grains which replace electrons as the principal destructors of D_3^+.

Figure 8 shows radial abundance profiles in a chemical model otherwise similar to the middle panel of Fig. 6, but for cosmic ionization rates $\zeta = 3 \times 10^{-18}$ s^{-1} and $\zeta = 3 \times 10^{-16}$ s^{-1}. It can be immediately seen in Fig. 8, as compared with the middle panel in Fig. 6, that the abundances of H^+ and H_3^+ follow the change in the cosmic ray ionization rate. The H^+ abundance is proportional to ζ via dissociation of H_2 by cosmic rays and via dissociative charge transfer reaction between He^+ and H_2 (see, e.g. Walmsley et al. 2004, Appendix A). The formation

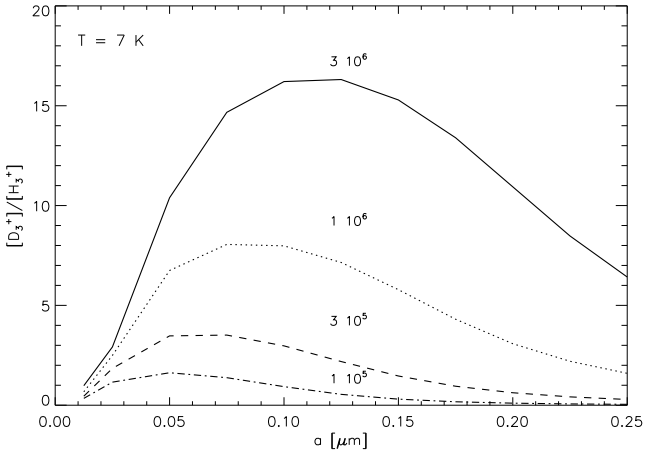

Fig. 9. Dependence of the D fractionation on the average grain size. The curves correspond to different values of the gas density.

of H_3^+ depends on ζ through H_2^+, which is the principal product of the collision between H_2 and a cosmic ray proton (e.g., Walmsley et al. 2004; Pagani et al. 2009). The H_2D^+ and D_2H^+ abundances are dragged upwards with H_3^+ with an intensified cosmic ray ionization, whereas the D_3^+ abundance remains roughly constant in the core center and falls off in the outer regions. So, quite reasonably, the $[D_3^+]/[H_3^+]$ ratio which depends on DR reactions diminishes strongly with an increasing ζ, whereas the effects on $[H_2D^+]/[H_3^+]$ and $[D_2H^+]/[H_3^+]$ which depend on HD and H_2(o/p), are less notable.

4.3. Molecular line profiles

The observed H_2D^+(o) profile from Oph D can be reproduced reasonably well using a hydrostatic core model together with the "complete depletion" chemistry model with the rate coefficients of Hugo et al. (2009) (see Fig. 10). The model giving the best agreement with the observed H_2D^+(o) spectrum (see Sect. 3.3) predicts a very weak D_2H^+(p) line at 692 GHz ($T_{\rm A}^* \sim 0.07$ K with APEX). This line has a lower peak opacity ($\tau \sim 0.6$) than the H_2D^+(o) line, whereas the radial $T_{\rm ex}$ distributions of the two lines are similar. One should note that even an optically thick D_2H^+(p) (1_{10}–1_{01}) line from a cold source is weak in the brightness temperature scale because the frequency lies far away from the range where the Rayleigh-Jeans approximation is valid.

The physical model adopted from Stark et al. (2004) (see Sect. 3.3) for the core I16293E produces easily the bright H_2D^+(o) and D_2H^+(p) lines observed by Vastel et al. (2004) (see Fig. 11, solid curves). The relatively high temperature (16–20 K) assumed by Stark et al. (2004) gives, however, rise to too broad lines as compared with the observations. Another problem with this assumption is that the chemistry model predicts a clearly higher D_2H^+(p)/H_2D^+(o) abundance ratio around 16 K (see Fig. 7 in Flower et al. 2004). We carried out another simulation assuming that the kinetic temperature is 10 K in the center and that it increases gradually to 12 K at the edge. The fractional H_2D^+(o) and D_2H^+(p) abundances were assumed to be roughly equal, in agreement with the prediction of the chemistry model. The modelled spectra are shown in Fig. 11 (dashed curves). Now both intensities and line widths are within the range reported by Vastel et al. (2004). The H_2D^+(o) and D_2H^+(p) column densities, both ~2.3×10^{-13} cm^{-2}, are slightly higher than those derived by Vastel et al. (2004).

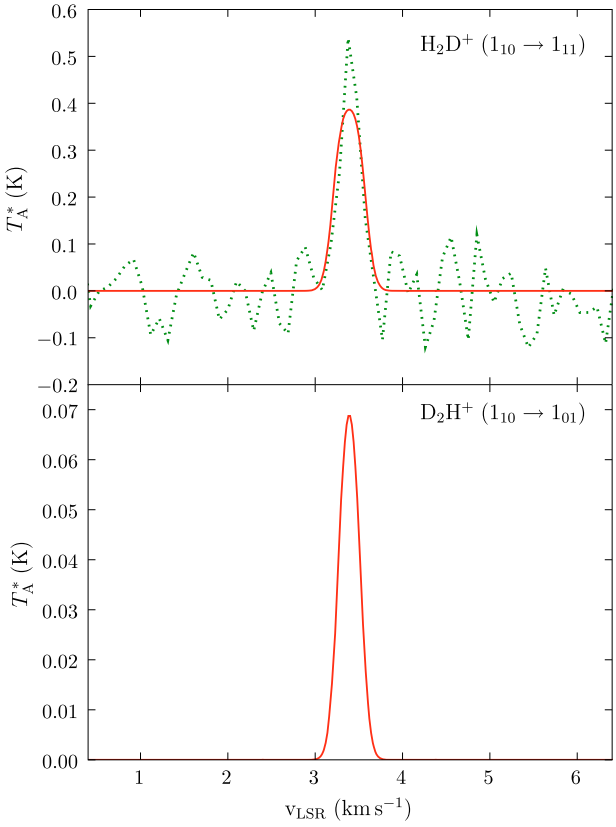

Fig. 10. Predicted line profiles for the H_2D^+ 1_{10}–1_{11} (ortho) and the D_2H^+ 1_{10}–1_{01} (para) transitions as observed with APEX for the best-fit core model (solid curves). Also plotted is the observation toward Oph D by Harju et al. (2008) for the H_2D^+ 1_{10}–1_{11} transition (dotted curve).

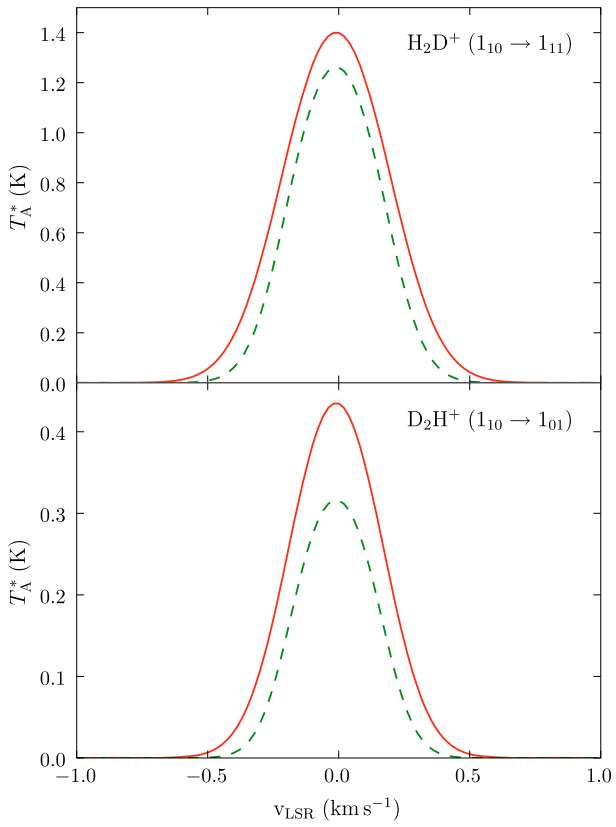

Fig. 11. Predicted molecular line profiles for the H_2D^+ (1_{10}–1_{11}) and the D_2H^+ (1_{10}–1_{01}) transitions for the prestellar core 16293E as observed with the CSO, using the core parameters of Stark et al. (2004) (solid curve). The modified model (see text) is also plotted (dashed curve).

5. Conclusions

We studied the chemistry in molecular cloud cores in the complete depletion limit, taking advantage of new state-to-state chemical reaction rate coefficients for the $H_3^+ + H_2$ reacting system (Hugo et al. 2009). We used the modelling results to predict line emission spectra for the H_2D^+ 1_{10}–1_{11} (372 GHz) and the D_2H^+ 1_{10}–1_{01} (692 GHz) transitions in a core model corresponding to the prestellar core Oph D. We also carried out simulations of the above transitions for the I16293E core. The simulated spectra were compared with observations by Harju et al. (2008) and Vastel et al. (2004) for the respective cores.

In this paper, we used steady-state chemical abundances in the molecular line simulations. It has been noted in the literature that the timescale for chemical development can be an order of magnitude larger than the dynamical timescale, and thus chemical steady-state might not be reached before collapse begins (see for example Flower et al. 2006). In general, however, ions reach chemical steady-state earlier than neutral species, due to the speed of the ion-molecule reactions. In fact, our chemical models indicate that ions reach steady-state before $t = 1 \times 10^5$ years. On the other hand, the relatively high H_2D^+(o) and D_2H^+(p) column densities derived toward Oph D and I16293E imply an appreciable degree of deuteration, which suggests that the cores are in an advanced chemical state. Taking into account these arguments, the assumption of steady-state seems, in the present context, appropriate.

The simulated profile of the H_2D^+ (1_{10}–1_{11}) line from a self-consistent hydrostatic core model (including chemistry modelling) is in reasonably good agreement with observations toward Oph D. The model predicts that the D_2H^+ (1_{10}–1_{01}) line at 692 GHz probably cannot be detected in this source. In fact, this transition is difficult to detect in emission in any cold object because of its high frequency. The same is true for the H_2D^+(p) and D_2H^+(o) ground state lines, which lie at even higher frequencies of ~1.4 THz.

The Oph D core seems particularly appropriate for using a hydrostatic model. However, the chemistry model used here begins to lose its validity in the outer parts, where the density drops below 10^6 cm^{-3}. In these conditions one can no longer ignore heavier substances in the gas phase, which modify the abundances of H_3^+ and its deuterated forms. So, in reality, the H_2D^+ and D_2H^+ abundances which in our models rise toward the core edge are likely to turn down outside the dense nucleus. This effect can be seen in the models of Pagani et al. (2009). It is obvious that chemical modelling should be extended to account for the presence of heavier species. This would also justify studies of larger cores, presenting larger density gradients.

Our simulations of molecular line profiles toward the I16293E core are in good agreement with the observational results presented in Vastel et al. (2004). While line emission simulations utilizing the physical core parameters of Stark et al. (2004) produce enough emission, we found that to produce linewidths comparable to those in Vastel et al. (2004), the core temperature profile and chemical abundances should be modified. This modification is also justified by results from chemical modelling. The H_2D^+(o) and D_2H^+(p) column densities are

found to become comparable when the temperature drops to ~10 K.

The deuteration of H_3^+ proceeds much faster in the present reaction scheme using the Hugo et al. (2009) results than in the Flower et al. (2004) model where the deuteration rate coefficients were adopted from Gerlich et al. (2002). As a consequence, the steady-state D_3^+/H_3^+ abundance ratio becomes larger than in the models of Flower, Pineau des Forêts & Walmsley. However, it should be noted that already in Walmsley et al. (2004), D_3^+ becomes the most abundant isotopologue of H_3^+ at very high densities, and that this phenomenon was predicted previously by Roberts et al. (2003).

The low-temperature rate coefficients from Gerlich et al. (2002) are lower than those by Hugo et al. (2009) by a factor of ~4. The experimental circumstances have been thoroughly discussed in Hugo et al. (2009), concluding that further experimental investigations, preferably with a different setup, are urgently needed. The ortho/para ratios of the deuterated forms of H_3^+ are also modified in the new model. Along with the changes in abundances, this has an impact on the observability of H_2D^+ and D_2H^+ toward prestellar cores. We find at very low temperatures a lower H_2D^+ (o/p) ratio, and a slightly higher D_2H^+ (p/o) ratio than predicted by using the coefficients adopted in Flower et al. (2004).

The state-to-state coefficients calculated by Hugo et al. (2009) provide an opportunity to refine both the chemistry model and the model for the excitation of the rotational transitions of interest. Besides collisions with *para* and *ortho* H_2, it would seem reasonable to examine the excitation of rotational levels of H_2D^+ and D_2H^+ in collisions with HD. The next step forward is to combine the full state-to-state reaction network with radiative transfer calculations. The realization of this improvement looks particularly feasible for the complete depletion model.

Acknowledgements. O.S. and J.H. acknowledge support from the Academy of Finland grant No. 117206. We would also like to thank D. Flower, G. Pineau des Forêts, C.M. Walmsley and L. Pagani for their comments on this paper, and the anonymous referee for his/her helpful report.

References

Amano, T., & Hirao, T. 2005, J. Mol. Spec., 233, 7
Bacmann, A., André, P., Puget, J.-L., et al. 2000, A&A, 361, 555
Bergin, E. A., & Tafalla, M. 2007, ARA&A, 45, 339
Bergin, E. A., Maret, S., van der Tak, F. F. S., et al. 2006, ApJ, 645, 369
Bonnor, W. B. 1956, MNRAS, 116, 351
Burke, J. R., & Hollenbach, D. J. 1983, ApJ, 265, 223
Caselli, P., van der Tak, F. F. S., Ceccarelli, C., & Bacmann, A. 2003, A&A, 403, L37
Caselli, P., Vastel, C., Ceccarelli, C., et al. 2008, A&A, 492, 703
Chapman, N. L., Mundy, L. G., Lai, S.-P., & Evans, N. J. 2009, ApJ, 690, 496
Draine, B. T., & Sutin, B. 1987, ApJ, 320, 803
Evans, II, N. J., Rawlings, J. M. C., Shirley, Y. L., & Mundy, L. G. 2001, ApJ, 557, 193
Flower, D. R., & Pineau des Forêts, G. 2003, MNRAS, 343, 390
Flower, D. R., Pineau des Forêts, G., & Walmsley, C. M. 2004, A&A, 427, 887
Flower, D. R., Pineau des Forêts, G., & Walmsley, C. M. 2006, A&A, 449, 621
Gerlich, D., Herbst, E., & Roueff, E. 2002, Planet. Space Sci., 50, 1275
Gould, R. J., & Salpeter, E. E. 1963, ApJ, 138, 393
Harju, J., Juvela, M., Schlemmer, S., et al. 2008, A&A, 482, 535
Herbst, E., & Klemperer, W. 1973, ApJ, 185, 505
Hily-Blant, P., Walmsley, M., Pineau Des Forêts, G., & Flower, D. 2008, A&A, 480, L5
Hollenbach, D., & Salpeter, E. E. 1971, ApJ, 163, 155
Hugo, E., Asvany, O., & Schlemmer, S. 2009, J. Chem. Phys., 130, 164302
Juvela, M. 1997, A&A, 322, 943
Juvela, M. 2005, A&A, 440, 531
Juvela, M., & Padoan, P. 2003, A&A, 397, 201
Li, A., & Draine, B. T. 2001, ApJ, 554, 778
Lombardi, M., Lada, C. J., & Alves, J. 2008, A&A, 480, 785
Mathis, J. S., Rumpl, W., & Nordsieck, K. H. 1977, ApJ, 217, 425
Miller, S., Tennyson, J., & Sutcliffe, B. 1989, Mol. Phys., 66, 429
Ossenkopf, V., & Henning, T. 1994, A&A, 291, 943
Pagani, L., Salez, M., & Wannier, P. G. 1992, A&A, 258, 479
Pagani, L., Vastel, C., Hugo, E., et al. 2009, A&A, 494, 623
Ramanlal, J., & Tennyson, J. 2004, MNRAS, 354, 161
Roberts, H., Herbst, E., & Millar, T. J. 2003, ApJ, 591, L41
Roberts, H., Herbst, E., & Millar, T. J. 2004, A&A, 424, 905
Stark, R., Sandell, G., Beck, S. C., et al. 2004, ApJ, 608, 341
van der Tak, F. F. S., Caselli, P., & Ceccarelli, C. 2005, A&A, 439, 195
Vastel, C., Phillips, T. G., & Yoshida, H. 2004, ApJ, 606, L127
Walmsley, C. M., Flower, D. R., & Pineau des Forêts, G. 2004, A&A, 418, 1035